Accepted Manuscript

Intrinsic and extrinsic doping contributions in SnO_2 and SnO_2:Sb thin films prepared by reactive sputtering

C. Guillén, J. Herrero

Please cite this article as: C. Guillén, J. Herrero, Intrinsic and extrinsic doping contributions in SnO_2 and SnO_2:Sb thin films prepared by reactive sputtering, *Journal of Alloys and Compounds* (2019), doi: https://doi.org/10.1016/j.jallcom.2019.03.302.

Intrinsic and extrinsic doping contributions in SnO$_2$ and SnO$_2$:Sb thin films prepared by reactive sputtering

C. Guillén* and J. Herrero

CIEMAT- Department of Energy, Avda. Complutense 40, Edif. 42, Madrid 28040, Spain.

*Corresponding author: c.guillen@ciemat.es, phone: +34-91-3466669.

Abstract: SnO$_2$ thin films are considered cheap transparent electrodes, interesting for scalable electronic applications, with intrinsic n-type conductivity related to donor defects like tin interstitials and oxygen vacancies. Besides, SnO$_2$ allows n-type extrinsic doping by pentavalent cations such as Ta or Sb. In the present work, SnO$_2$ and SnO$_2$:Sb films were deposited on unheated soda lime glass substrates by reactive DC sputtering from Sn and Sn:Sb(5%) targets. Their structural, optical and electrical properties have been analyzed comparatively for the layers prepared at different oxygen partial pressures in the sputtering atmosphere, as-grown and after heating in air at several temperatures. Sb doping is proven effective to improve the electrical conductivity of sputtered tin dioxide samples. The contribution of oxygen vacancies is found dependent on the reactive deposition environment, in both pure and Sb-doped films, but subsequent heating can change the proportion and nature of the donor defects. For operation at temperatures above 400 ºC, SnO$_2$:Sb shows the best electrical performance and good thermal behavior is also achieved with pure SnO$_2$ layers by adjusting the oxygen content in the sputtering atmosphere.

Keywords: A: oxide materials, thin films; C: electronic properties, optical properties.

1. Introduction

Tin dioxide is a semiconductor material widely used in various applications, including solar energy conversion, catalysis or gas sensing [1–3]; and particularly suitable as transparent electrode in thin-film optoelectronic devices [4]. This is due to its high optical transmittance, with a large band-gap above 3.6 eV, and intrinsic n-type conductivity related to a low formation energy for tin interstitials (Sn$_i$) and oxygen vacancies (V$_O$) acting as donor defects [5]. Taking into account the dual valence of tin, theoretical calculations have given lower formation energy for V$_O$ than Sn$_i$. They predict that oxygen vacancies, compensated by some Sn reduction, are the most abundant intrinsic defect under oxygen poor conditions, which lead to conductivity through the mobility of electrons from Sn(II) to Sn(IV) sites [6]. Nevertheless, tin interstitials have been found predominant in some experimental conditions. For example, in SnO$_2$ thin films obtained by oxidation of evaporated metal layers [7]. Also, in SnO$_2$ samples prepared by pulsed laser

1

deposition, the dominant defect was observed to change from Sn_i to V_O when the background oxygen pressure was increased [8].

The highest conductivity values achieved by intrinsic doping in SnO_2 layers are within the 10-10^2 S/cm range [9–12]. In order to improve these intrinsic values, several pentavalent cations have been tested as extrinsic dopants in SnO_2, being Sb the most used because its ability to increase the electrical conductivity maintaining a high optical transmittance [13]. A small proportion of Sb (Sb/Sn = 2-10% at.) can rise the conductivity of SnO_2:Sb films to the 10^2-10^3 S/cm range [12,14–17]. Usually, post-deposition annealing in air at high temperature (400-600 ^{o}C) is needed to achieve the best performance, by increasing the proportion of Sb(V) placed in substitutional sites (Sb_{Sn}) and reducing defects at the grain boundaries [17,18]. For as-grown and heated SnO_2:Sb samples, there is also some dependence of the electrical conductivity on the oxygen content in the deposition atmosphere [14,15], analogous to that observed for pure SnO_2 layers [9,10]. This indicates that intrinsic donor defects (V_O and/or Sn_i) can contribute in the same order than the extrinsic ones (Sb_{Sn}) to the overall conductivity of SnO_2:Sb thin films [19].

Annealing treatments are often employed to enhance the optical and electrical properties of transparent electrodes to be applied in optoelectronic devices [20–22]. Furthermore, heat-resistant properties are required to prevent the adverse effects of high-temperature processes during the device fabrication and/or operation [23,24]. Several studies have proven that SnO_2 and SnO_2:Sb layers have better thermal stability than analogous transparent electrodes consisting of ZnO or In_2O_3 compounds [25,26]. However, it should be noted that the effects of thermal annealing can be highly dependent on the initial characteristics of the metal oxide films [20,21].

Here we present a comparative study of SnO_2 and SnO_2:Sb layers prepared by reactive DC magnetron sputtering from Sn and Sn:Sb(5%) metallic targets, varying the oxygen to argon partial pressure ratio to promote the formation of donor defects. The structural, optical, and electrical properties have been investigated for the as-grown films on unheated glass substrates and after annealing in air at various temperatures from 150 to 500 ºC. The principal objective has been to determine the best deposition parameters to achieve layers with high visible transparency and n-type conductivity that remain stable for high-temperature operations. The results obtained can contribute to the expansion of tin dioxide coatings as cheap and stable transparent electrodes for multiple electronic applications.

2. Experimental details

Metal oxide thin films were prepared by reactive DC magnetron sputtering on unheated soda-lime glass substrates. The targets were discs of Sn (purity 99.99%) and Sn:Sb (5% Sb, purity 99.99%) of 15 cm diameter, which were used for deposition of SnO_2 and SnO_2:Sb layers,

respectively. After evacuation of the chamber to a base pressure of $4*10^{-4}$ Pa, oxygen and argon gases were introduced by independent mass flow controllers. The argon flow was fixed at 60 sccm, resulting in a change to 0.4 Pa, whereas the oxygen flow was varied to achieve different oxygen partial pressures (O_{pp}). Then, a DC power of 200 W was applied to the target, resulting in current and voltage values that depend on the oxygen ratio, as it is illustrated in Fig. 1. When $O_{pp} \leq 18\%$, an almost constant high voltage is achieved, this indicating that the sputtering process operates in the metallic mode [27]. The transition towards the oxide mode is detected by the voltage decrease when the oxygen proportion increases above 18% O_{pp}. Transparent and conductive films have been obtained in the transition region O_{pp}= 18-24%, where both Sn and Sn:Sb targets gave similar voltage values. At higher oxygen ratios, $O_{pp} > 24\%$, the self-bias voltage decreases faster for Sn than Sn:Sb, which is attributed to a relatively faster oxidation of the pure Sn target surface. For layers prepared at different conditions, a same thickness of 0.2 µm has been used for comparison. Post-deposition annealing of the samples was performed in air at temperatures ranging from 150 to 500 °C during 30 minutes.

The microstructure of the films was analyzed with a B&W Tek system composed of BAC151B microscope and i-Raman spectrometer, using a green laser of 532 nm as the excitation source. The crystallographic properties were also examined by X-ray diffraction (XRD) with radiation Cu Ka1 (λ = 1.54056 Å) in a Philips X'pert instrument with Bragg-Brentano θ-2θ configuration. Crystalline phases have been identified with the cards given by the Joint Committee of Powder Diffraction Standards (JCPDS). The mean crystallite size is calculated from the full width at half maximum of the main diffraction peak, according to the Scherrer formula.

Optical transmittance (T) and reflectance (R) measurements were done with a double beam spectrophotometer Perkin-Elmer Lambda 9 at wavelengths from 300 to 1500 nm, taking the air as reference. In order to eliminate the interference peaks, the transmittance is corrected for reflection losses [28,29]: $T_c(\%) = 100\ T(\%)/(100 - R(\%))$. Then, the optical absorption coefficient is calculated as $\alpha = (1/t)\ ln[100/T_c(\%)]$, including the film thickness value (t) obtained by profilometry with a Dektak 3030. The band-gap energy (E_g) has been calculated according to direct transitions: $\alpha = A(h\nu - E_g)^{1/2}$ [19][10]. For electrical characterization, the conductivity together with carrier concentration and mobility were determined with an ECOPIA system based on Hall-effect measurements.
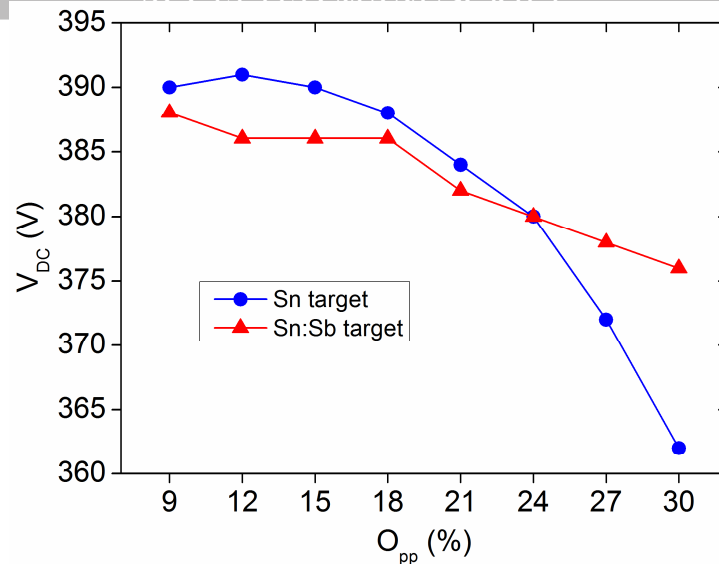
Fig. 1. Variation in the target self-bias as a function of the oxygen partial pressure during the reactive sputtering.

3.   Results and discussion

All the films grown in the present experimental conditions have poor crystallinity, since no peaks of oxide compounds appear in the X-ray diffractograms. Nevertheless, some information about the microstructure of the as-deposited layers has been obtained from the Raman spectra displayed in Fig. 2. When the oxygen ratio was set at 18% O_{pp}, the formation of SnO_2 is detected by the increment of the Raman intensity in the 400-800 cm^{-1} region. Effectively, for tetragonal SnO_2 with poor crystallinity, the classical vibration modes Eg (476 cm^{-1}), A1g (638 cm^{-1}) and B2g (782 cm^{-1}) can be together with three wide bands S1 (centered around 570 cm^{-1}), S2 (~500 cm^{-1}) and S3 (~700 cm^{-1}) that appear as a consequence of disorder activation [30,31]. The deconvolution of the experimental spectrum in Fig. 2 shows the presence of Eg and A1g modes as well as S1 and S3 bands, without significant changes between the SnO_2 and SnO_2:Sb films prepared at 18% O_{pp}. For these samples, the Raman intensity increases also in the 75-200 cm^{-1} range, where several vibrational modes for SnO and intermediate oxides SnO_x (including Sn_2O_3 and Sn_3O_4) can be located [32,33]. Otherwise, no evidence of SnO_x or SnO_2 is found for the layers prepared at 24% O_{pp}, this suggesting that the microstructural order decreases for higher oxygen proportions.
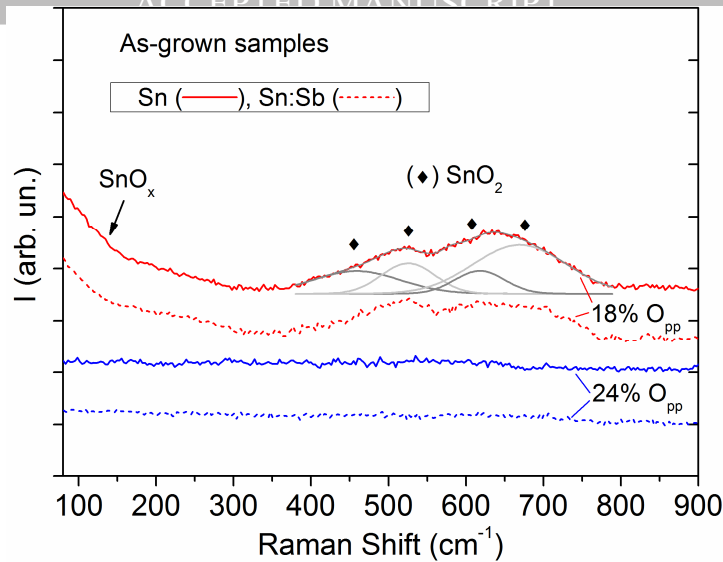
4

Fig. 2. Raman spectra corresponding to the films deposited by reactive sputtering at different oxygen partial pressures from Sn and Sn:Sb targets.

Fig. 3 illustrates the influence of the preparation conditions (target composition and oxygen partial pressure) on the optical characteristics of the metal oxide films. In order to compare the various samples, the average transmittance in the visible spectral range (λ = 400-800 nm) has been calculated and summarized in Table 1. The highest visible transmittance corresponds to the layer obtained at 24% O_{pp} from the Sn target (T_{vis} = 97%), decreasing slightly for the analogous sample including Sb (T_{vis} = 91%). A progressive decrease in the visible transmittance has been reported for SnO_2:Sb thin films with increasing Sb content [34–36], which has been attributed to the ready excitation of additional electrons provided in the SnO_2 matrix by the Sb ions [34]. Otherwise, the layers prepared at 18% O_{pp} show a further decrease in the visible transmittance (83% and 70% for the Sn and Sn:Sb targets, respectively). This is related to the displacement of the absorption edge towards higher wavelengths (lower radiation energies) when the oxygen partial pressure was decreased. The band-gap energy E_g, as calculated in the Fig. 3 inset, changes from 2.96 eV and 2.68 eV, for the pure and Sb-doped layers deposited at 18% O_{pp}, to 3.70 eV and 3.74 eV, for the analogous films prepared at 24% O_{pp}. The experimental data included in Table 1 evidence that such band-gap widening goes together with a significant increment in the electrical conductivity due to a rise in the carrier concentration (ΔN $\sim 10^5$). Thus, the amorphous samples obtained at the highest oxygen proportion show characteristics of SnO_2 (E_g > 3.6 eV), with a considerable concentration of free electrons when sputtered from the Sn target ($5.1*10^{17}$ cm^{-3}) and higher by including Sb ($4.9*10^{19}$ cm^{-3}), which gives a maximum conductivity σ = 8.8 S/cm for the as-grown films. Otherwise, the layers prepared at a lower oxygen pressure are dominated by SnO-like characteristics, with a narrower band-gap and a low concentration of free electrons, even by using the Sn:Sb target. Similar

5

behavior has been observed in other works, where small variations in the oxygen content produce great changes in the electrical conductivity, with $\Delta\sigma \sim 10^5$ for $\Delta O_{pp} < 5\%$ in pure and Sb-doped tin oxide films [14,37].
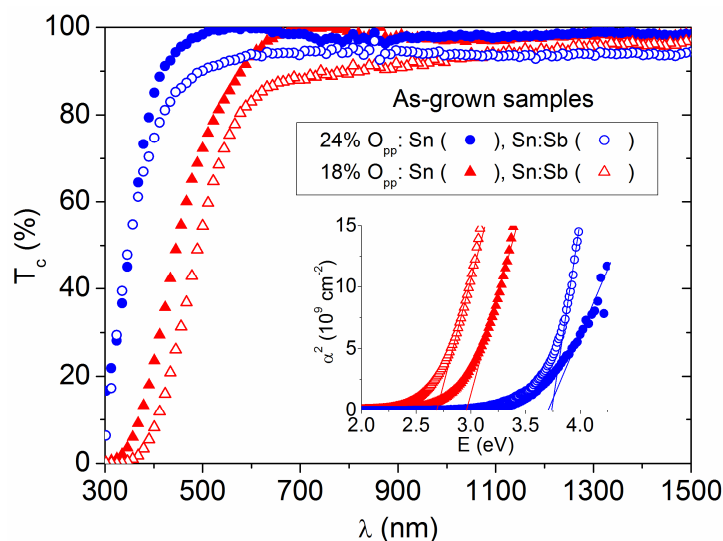

Fig. 3. Optical transmittance data obtained for the films grown at different oxygen partial pressures from Sn and Sn:Sb targets. The inset shows the band-gap energy calculation.

The as-grown amorphous samples crystallized in the cassiterite SnO_2 phase after heating in air at $T \geq 400$ ºC. These crystalline layers exhibit diffraction peaks from the (110), (101), (200) and (211) planes according to the standard tetragonal SnO_2 structure (JCPDS card No 41-1445). Fig. 4 shows the evolution with the annealing temperature of the XRD patterns of tin oxide films deposited at 18% O_{pp} from the Sn target. These preparation conditions have resulted in the highest crystallization after heating, giving a maximum crystallite size of 14 nm at 450 ºC. For the rest of the samples, the mean size is about 6-8 nm, in the same range than reported for tin oxide films prepared by reactive sputtering on heated substrates [10]. The limited crystallite growth is related to intrinsic defects caused by vacancies and/or interstials, and additional defects created by the Sb dopant into the SnO_2 lattice [17,34]. The most crystalline layer evidences also the formation of some Sn_2O_3 (JCPDS card No 25-1259) and Sn_3O_4 (JCPDS card No 20-1293). These have triclinic structures that are theoretically formed when some layers of oxygen are removed from (101) planes of rutile SnO_2 [38]. They consist of SnO_2-like local structures in which Sn is quadrivalent together with SnO-like structures where it is divalent [39]. Such intermediate oxides can crystallize within oxygen-deficient SnO_2 lattices when the formation of oxygen vacancies and/or tin interstitials defects enables the reduction of some Sn^{4+} ions to Sn^{2+} as a possible charge compensation mechanism [6].
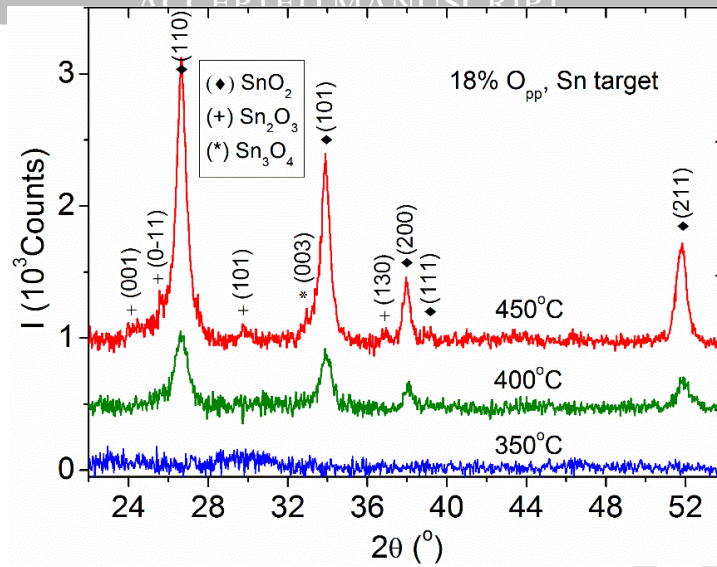
Fig. 4. XRD patterns corresponding to tin oxide layers prepared at 18% O_{pp} from the Sn target and subsequently heated in air at different temperatures.

The influence of the preparation conditions on the crystalline SnO_2 features is illustrated in Fig. 5 for the various samples that were heated at 450 ºC. The diffraction peaks of the layers prepared from the Sn target show intensities ratios that are according to the SnO_2 powder standard for $I(110)/I(101) \sim 1.4$ and $I(110)/I(200) \sim 4.9$, but $I(211)$ is below that expected from the standard ratio $I(110)/I(211) = 1.7$. Otherwise, the analogous layers obtained from the Sn:Sb target exhibit a significant increment of the (101) and (211) orientations. A similar change toward preferred (101) orientation has been observed for other polycrystalline SnO_2 and SnO_2:Sb films prepared by reactive sputtering at low oxygen pressures [10,40]. Here, the enhancement of the (101) diffraction detected for the Sb-doped samples is attributed to the ingress of some Sb^{3+} substituting Sn^{4+} in the lattice, which can create additional oxygen vacancies for charge compensation [19]. An increase of the unit cell could be expected due to cationic repulsion associated with oxygen vacancies and also because of the largest ionic radii for Sb^{3+} (0.076 nm) than Sn^{4+} (0.069 nm) [19]. Nevertheless, some decrease of the (101) interplanar distance is detected for the present SnO_2:Sb samples ($d_{101} = 0.262$ nm) in comparison with the standard value obtained for the SnO_2 films ($d_{101} = 0.264$ nm). This is thought to be due to the prevalence of Sb^{5+}, which has a lower ionic radius ~ 0.062 nm that helps its entrance into the SnO_2 lattice and reduces the unit cell dimensions [36]. Besides, a high (211) diffraction, corresponding to a surface grain orientation between (101) and (110), has been related to an optimal Sb incorporation at substitutional positions [16,41,42]. In this sense, the incorporation seems to be better for the layer prepared from Sn:Sb at 24% O_{pp}, which exhibits the highest (211) diffraction and also maximum carrier concentration (in Table 1).
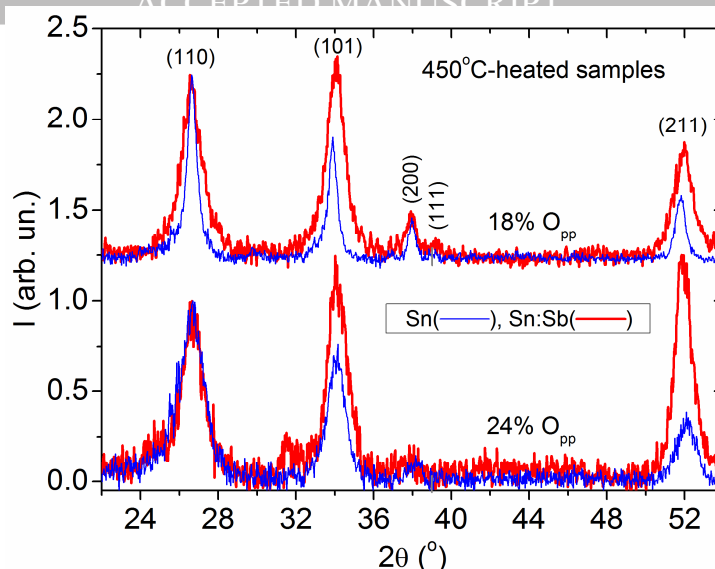
7

Fig. 5. SnO_2 diffraction peaks for the tin oxide layers deposited at various conditions and subsequently heated in air at 450 ºC.

The Raman spectra reveal also microstructural changes for the various tin oxide films after heating at 450 ºC, as illustrated in Fig. 6. This shows SnO_2 signals with low intensity and broad width, indicating that a high structural disorder remains in these samples with small crystallites. The fundamental mode A1g (638 cm^{-1}) is detected together with the disorder-activated bands S2 (~500 cm^{-1}) and S3 (~700 cm^{-1}) [30], which are identified by deconvolution of the Raman signal for the layers deposited at 24% O_{pp}. The same bands are observed in the films prepared at 18% O_{pp}, but with a relatively smaller width that makes possible their identification without deconvolution. For the samples prepared at the lowest oxygen ratio, the subsequent heating evidences additional peaks at low wave numbers, which are attributed to Sn_3O_4 (with Raman-active modes at 90, 140, 170 and 240 cm^{-1} [33,43]) and Sn_2O_3 (with vibrational frequencies at 122 and 155 cm^{-1} [33]). Although these intermediate oxides have already been noted in the corresponding XRD diagram of Fig. 4, their presence is more evident in the Raman spectra, which allow determining the preferred formation of Sn_3O_4 or Sn_2O_3 for the pure or Sb-doped layers, respectively. Both intermediate oxides are thermodynamically stable and can be transformed into each other by a small variation in the oxygen and/or tin chemical potentials [39]. By considering a fixed chemical potential for oxygen, the prevalence of Sn_2O_3 indicates a certain increment in the chemical potential for tin in the Sb-doped samples.
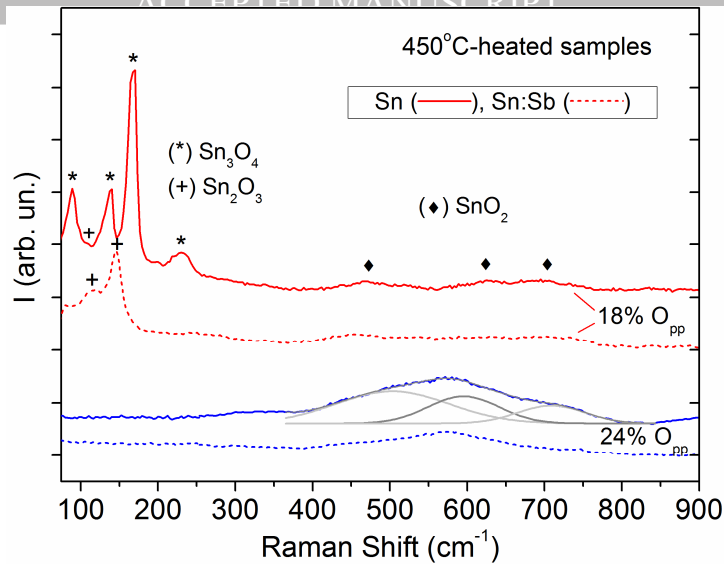
Fig. 6. Raman spectra for the tin oxide samples deposited at various conditions and subsequently heated in air at 450 ºC.

The optical properties of the crystallized films are represented in Fig. 7, for the layers prepared at various experimental conditions and subsequently heated in air at 450 ºC. The comparison with the as-grown characteristics (Fig. 3) evidences that heating produces band-gap widening and subsequent increment in the visible transmittance for each sample, which is commonly associated with the elimination of structural defects during the crystallization process [16]. Nevertheless, it remains some influence of the deposition conditions on the optical characteristics of the annealed films. The gap energy continues below 3.6 eV for the layers prepared at 18% O_{pp} and the visible transmittance is lower for the samples containing Sb. The differences observed after heating are $\Delta T_{vis} \sim$ 5-10 % with respect to the analogous films obtained from pure Sn target, maintaining the proportion observed in the as-grown conditions.
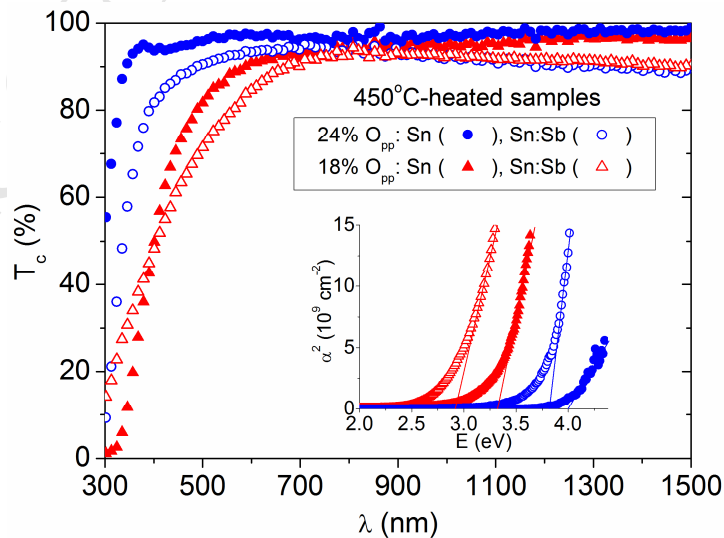

Fig. 7. Optical data for the tin oxide films prepared at different conditions and heated at 450 ºC. The inset shows the band-gap energy calculation.

9

Fig. 8 summarizes the optical characteristics of the tin oxide layers prepared at different conditions, before and after heating in air at the various temperatures. For pure and Sb-doped samples, the visible transmittance and band-gap energy are always lower when they are deposited at 18% O_{pp}. These layers contain Sn_3O_4 and/or Sn_2O_3 together with the main SnO_2 phase, as proven by the corresponding XRD patterns and Raman spectra. Such intermediate oxides are responsible for the relatively small band gap achieved (< 3.4 eV), which is in the same order than reported for other mixed-phase samples [39,44]. Otherwise, the layers deposited at 24% O_{pp} evidence wide band gaps in the 3.6-4.1 eV range, typical of single-phase SnO_2 films [10,44,45]. For highly doped semiconductors, the variation in the optical energy gap may arise from two different mechanisms. One is the Moss–Burstein shift, which predicts an effective gap widening $E_g = E_{g0} + (\hbar^2/2m^*)(3\pi^2N)^{2/3}$ in relation to the undoped standard value (E_{g0}) when the carrier concentration (N) increases [46]. Such band-gap widening applies generally for carrier concentrations in the 10^{18}-10^{19} cm^{-3} range [10,45,47], as shown in the Fig. 8 inset for the films prepared at 18% O_{pp}. At superior carrier densities (10^{20}-10^{21} cm^{-3}) an opposite trend can be observed [48] due to the change from semiconductor to metallic behavior, with a dependence in the form $E_g = E_{g0} – (e^2/2\varepsilon)(3N/\pi^4)^{1/3}$ [46]. This other mechanism explains the band-gap shrinkage detected in the samples with the highest carrier concentrations, as it is illustrated in the Fig. 8 inset for the layers deposited at 24% O_{pp}. The fits plotted in the inset correspond to a carrier effective mass $m^* = 0.2\ m_0$ and permittivity $\varepsilon = 3\varepsilon_0$, with m_0 the electron rest mass and ε_0 the vacuum permittivity, according to the values determined for similar tin oxide films [49].
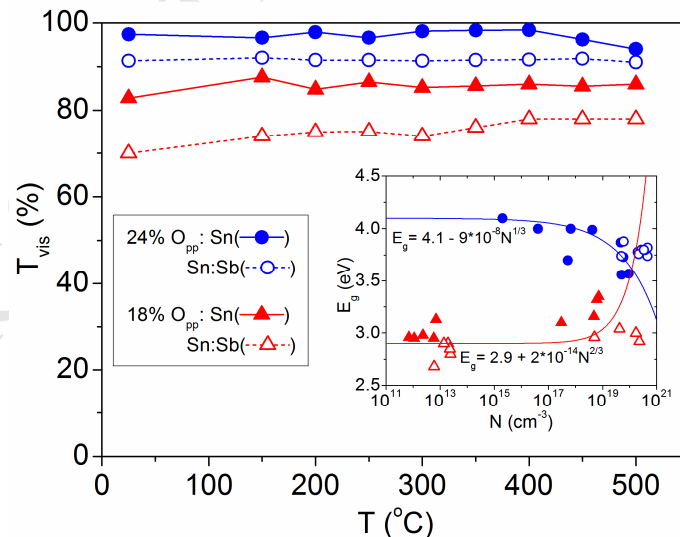

Fig. 8. Evolution of the visible transmittance with the heating temperature for the tin oxide layers prepared at different conditions. The inset shows the gap energy as a function of the carrier concentration for these samples.

The influence of the heating temperature on the electrical properties is described in Fig. 9. For the single-phase layers prepared at 24% O_{pp}, a conductivity maximum is achieved after annealing around 250 ºC, which is considered a critical temperature to change the air-sample interaction from oxygen desorption (V_O creation) to oxygen adsorption (V_O extinction) [50,51]. Then, a progressive conductivity decrease is observed for the pure SnO_2 films as the heating temperature increases above 250 ºC. Nevertheless, for the SnO_2:Sb layers the maximum conductivity remains practically unchanged up to 500 ºC. This is because extrinsic doping allows the formation of additional defects (substitutional Sb_{Sn} and interstitial Sb_i) more stable than the oxygen vacancies [12]. A different behavior is observed in the layers prepared at 18% O_{pp}, for which cation interstitials can become predominant due to the presence of Sn_3O_4 and Sn_2O_3 intermediate oxides. Indeed, theoretical and experimental investigations have demonstrated that metallic segregation occurs at the SnO/SnO_2 interface in mixed-phase samples [52–54]. The coexistence of disordered SnO-like and SnO_2-like structures causes the low conductivity values obtained for the as-grown films; but their crystallization above 400 ºC allows achieving high conductivities for the layers with and without Sb, which is attributed to the activation of cation interstitials (Sb_i and Sn_i) in addition to the substitutional Sb_{Sn}.
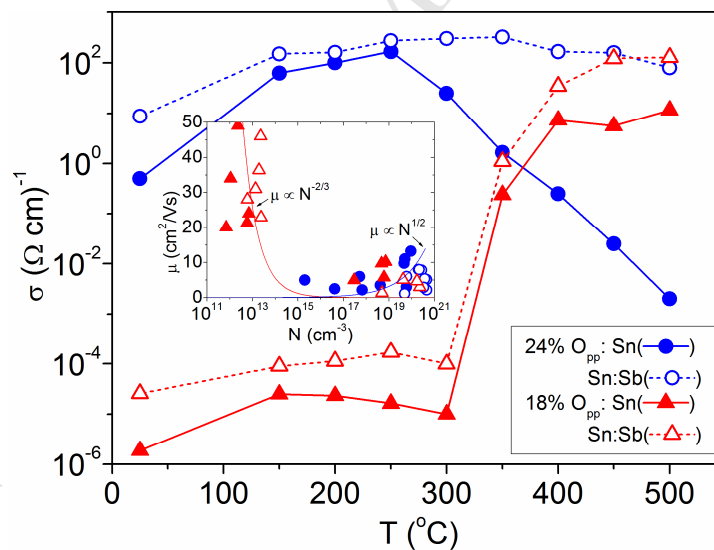
Fig. 9. Evolution of the electrical conductivity with the heating temperature for the tin oxide layers prepared at different conditions. The inset shows the mobility as a function of the carrier concentration for the same samples.

The effectiveness of the extrinsic doping is proven, because the tin oxide films containing Sb show higher carrier concentration and conductivity than the analogous layers prepared from the pure Sn target (in Table 1). The relation between the maximum carrier density ($N = 4.6*10^{20}$ cm^{-3}) and the Sb concentration ($c = 1.4*10^{21}$ cm^{-3}) gives a dopant activation efficiency $N/c = 33$

%, in the same order than reported for other SnO$_2$:Sb layers prepared by reactive sputtering on substrates heated at 450 ºC [55]. Here, the extrinsic dopant efficiency is found maximum after annealing above 400 ºC, when the films crystallize in the cassiterite SnO$_2$ phase, and the substitutional Sb$_{Sn}$ incorporation is related to an enhancement in the (211) diffraction (Fig. 5). For samples prepared from the pure Sn target, a relative maximum in the carrier concentration (9.2*10^{19} cm^{-3}) is achieved by deposition at 24% O$_{pp}$ and heating at 250 ºC. Similar carrier densities have been attributed to intrinsic doping by oxygen vacancies in non-stoichiometric SnO$_{2-\delta}$ films [9–11], taking into account that a small oxygen deficiency ($\delta \sim 1*10^{-3}$) can give a great conductivity enhancement ($\Delta\sigma \sim 10^4$) [56]. For the layers prepared at 18% O$_{pp}$, high carrier concentrations (10^{18}-10^{20} cm^{-3}) are also attained after heating above 400 ºC, because analogous carrier densities can be obtained with either oxygen vacancies or cation interstitials defects [8], but they have a different thermal stability.

The representation of the mobility as a function of the carrier concentration (in the Fig. 9 inset) has been used to identify the conduction mechanisms in these tin oxide films. For highly doped semiconductors, the electrical transport is usually dominated by ionized impurity scattering. The lattice ions, needed to balance the free carriers charge, make to decrease the mobility with increasing carrier density in the form $\mu \propto N^{-2/3}$ [57,58]. Such trend is observed for the present samples when $N \leq 10^{18}$ cm^{-3}, but at higher carrier densities some increment in the mobility is detected (Fig. 9 inset). At very high electron concentrations, the lattice ions can be screened [50] and the ionized impurity scattering becomes different. Besides, phonon scattering tends to decrease at high carrier densities [59], with a dependence $\mu \propto N^{1/2}$ that is observed for highly doped materials with metallic character [60].

4. Conclusions

SnO$_2$ and SnO$_2$:Sb thin films have been prepared by reactive sputtering from Sn and Sn:Sb(5%) targets, respectively, changing their properties by the oxygen partial pressure during growth on unheated substrates and by posterior annealing in air.

The as-grown samples have poor crystallinity, but a good combination of transparency and n-type conductivity is attained at 24% O$_{pp}$, where the Sb-doping increases the carrier concentration from 5.1*10^{17} to 4.9*10^{19} cm^{-3} and decreases the average visible transmittance from 97 to 91%. The electrical conductivity enhances by heating up to 250ºC, after which similar carrier densities are obtained for both SnO$_2$ (9.2*10^{19} cm^{-3}) and SnO$_2$:Sb (2.1*10^{20} cm^{-3}) due to the contribution of intrinsic doping by oxygen vacancies. These lessen by oxygen adsorption at higher temperatures, decreasing the carrier concentration in SnO$_2$, but not in SnO$_2$:Sb owing to the permanence of more stable extrinsic defects like Sb$_{Sn}$ and Sb$_i$. In fact, the maximum carrier

concentration ($4.6*10^{20}$ cm^{-3}) is achieved for the SnO$_2$:Sb films deposited at 24% O$_{pp}$ and annealed above 400 ºC, when they crystallize in the cassiterite SnO$_2$ phase with a preferential (211) orientation that indicates substitutional Sb$_{Sn}$ incorporation. The visible transmittance of these samples remains above 91 % after heating.

The transparency and conductivity of the as-grown films get worse by decreasing the oxygen ratio to 18% O$_{pp}$, because this allows the reduction of some Sn^{4+} to Sn^{2+}, which results in band-gap narrowing and compensation of oxygen vacancies. The coexistence of disordered SnO-like and SnO$_2$-like structures leaves few free electrons ($\sim 10^{12}$ cm^{-3}), but a significant enhancement is obtained after heating above 400 ºC, when SnO$_2$ crystallizes together with intermediate oxides Sn$_3$O$_4$ and/or Sn$_2$O$_3$. Then, high carrier concentrations and conductivities are achieved for the films with or without Sb ($2.3*10^{20}$ and $6.1*10^{18}$ cm^{-3}, respectively), which is attributed to the activation of cation interstitials (favored at the intermediate oxide interfaces) in addition to the substitutional Sb$_{Sn}$. In these conditions, the Sb-doping is also effective to enhance the conductivity but makes to decrease the average visible transmittance from 86 to 78%.

Declarations of interest: none.

References

[1] S. Lu, Y. Zhao, C. Chen, Y. Zhou, D. Li, K. Li, W. Chen, X. Wen, C. Wang, R. Kondrotas, N. Lowe, J. Tang, Sb$_2$Se$_3$ thin-film photovoltaics using aqueous solution sprayed SnO$_2$ as the buffer layer, Adv. Electron. Mater. 4 (2018) 1–8. doi:10.1002/aelm.201700329.

[2] R. Daiyan, X. Lu, W.H. Saputera, Y.H. Ng, R. Amal, Highly selective reduction of CO$_2$ to formate at low overpotentials achieved by a mesoporous tin oxide electrocatalyst, ACS Sustain. Chem. Eng. 6 (2018) 1670–1679. doi:10.1021/acssuschemeng.7b02913.

[3] K. Suematsu, N. Ma, K. Watanabe, M. Yuasa, T. Kida, K. Shimanoe, Effect of humid aging on the oxygen adsorption in SnO$_2$ gas sensors, Sensors (Switzerland). 18 (2018) 1–11. doi:10.3390/s18010254.

[4] M. Morales-Masis, S. De Wolf, R. Woods-Robinson, J.W. Ager, C. Ballif, Transparent electrodes for efficient optoelectronics, Adv. Electron. Mater. 3 (2017). doi:10.1002/aelm.201600529.

[5] C. Kílíç, A. Zunger, Origins of coexistence of conductivity and transparency in SnO_2, Phys. Rev. Lett. 88 (2002) 95501. doi:10.1103/PhysRevLett.88.095501.

[6] K.G. Godinho, A. Walsh, G.W. Watson, Energetic and electronic structure analysis of intrinsic defects in SnO_2, J. Phys. Chem. C. 113 (2009) 439–448. doi:10.1021/jp807753t.

[7] H. Sefardjella, B. Boudjema, A. Kabir, G. Schmerber, Structural and photoluminescence properties of SnO_2 obtained by thermal oxidation of evaporated Sn thin films, Curr. Appl. Phys. 13 (2013) 1971–1974. doi:10.1016/j.cap.2013.08.017.

[8] Y. Porte, R. Maller, H. Faber, H.N. AlShareef, T.D. Anthopoulos, M.A. McLachlan, Exploring and controlling intrinsic defect formation in SnO_2 thin films, J. Mater. Chem. C. 4 (2016) 758–765. doi:10.1039/C5TC03520A.

[9] C. Kim, S. Kim, S.E. Kim, Transparent SnO_x thin films fabricated by radio frequency reactive sputtering with a SnO/Sn composite target, Thin Solid Films. 634 (2017) 175–180. doi:10.1016/j.tsf.2017.02.045.

[10] S. Bansal, D.K. Pandya, S.C. Kashyap, D. Haranath, Growth ambient dependence of defects, structural disorder and photoluminescence in SnO_2 films deposited by reactive magnetron sputtering, J. Alloys Compd. 583 (2014) 186–190. doi:10.1016/j.jallcom.2013.08.135.

[11] S.S. Lin, Y.S. Tsai, K.R. Bai, Structural and physical properties of tin oxide thin films for optoelectronic applications, Appl. Surf. Sci. 380 (2016) 203–209. doi:10.1016/j.apsusc.2016.01.188.

[12] W. Mao, B. Xiong, Y. Liu, C. He, Correlation between defects and conductivity of Sb-doped tin oxide thin films, Appl. Phys. Lett. 103 (2013). doi:10.1063/1.4816084.

[13] S.C. Dixon, D.O. Scanlon, C.J. Carmalt, I.P. Parkin, n-Type doped transparent conducting binary oxides: an overview, J. Mater. Chem. C. 4 (2016) 6946–6961. doi:10.1039/C6TC01881E.

[14] J. Montero, C. Guillén, J. Herrero, Nanocrystalline antimony doped tin oxide (ATO) thin films: A thermal restructuring study, Surf. Coatings Technol. 211 (2012) 37–40. doi:10.1016/j.surfcoat.2011.07.068.

[15] W. Yang, S. Yu, Y. Zhang, W. Zhang, Properties of Sb-doped SnO_2 transparent conductive thin films deposited by radio-frequency magnetron sputtering, Thin Solid Films. 542 (2013) 285–288. doi:10.1016/j.tsf.2013.06.077.

[16] H. Zheng, L. Li, Z. Sun, S. Yu, W. Luo, Preferential orientation, microstructure and functional properties of SnO_2:Sb thin film: The effects of post-growth annealing, Appl. Surf. Sci. 362 (2016) 230–236. doi:10.1016/j.apsusc.2015.11.230.

[17] M. Zheng, J. Ni, F. Liang, M.C. Wang, X. Zhao, Effect of annealing temperature on the

crystalline structure, growth behaviour and properties of SnO$_2$:Sb thin films prepared by radio frequency (RF)-magnetron sputtering, J. Alloys Compd. 663 (2016) 371–378. doi:10.1016/j.jallcom.2015.12.037.

[18] W. Mao, B. Xiong, Q. Li, Y. Zhou, C. Yin, Y. Liu, C. He, Influences of defects and Sb valence states on the temperature dependent conductivity of Sb doped SnO$_2$ thin films, Phys. Lett. Sect. A Gen. At. Solid State Phys. 379 (2015) 1946–1950. doi:10.1016/j.physleta.2015.06.033.

[19] S. Haireche, A. Boumeddiene, A. Guittoum, A. El Hdiy, A. Boufelfel, Structural, morphological and electronic study of CVD SnO$_2$:Sb films, Mater. Chem. Phys. 139 (2013) 871–876. doi:10.1016/j.matchemphys.2013.02.046.

[20] P. Barquinha, G. Gonçalves, L. Pereira, R. Martins, E. Fortunato, Effect of annealing temperature on the properties of IZO films and IZO based transparent TFTs, Thin Solid Films. 515 (2007) 8450–8454. doi:10.1016/j.tsf.2007.03.176.

[21] C. Guillén, J. Herrero, Structure, optical, and electrical properties of indium tin oxide thin films prepared by sputtering at room temperature and annealed in air or nitrogen, J. Appl. Phys. 101 (2007) 73514. doi:10.1063/1.2715539.

[22] J.W. Leem, J.S. Yu, Physical properties of electrically conductive Sb-doped SnO$_2$ transparent electrodes by thermal annealing dependent structural changes for photovoltaic applications, Mater. Sci. Eng. B Solid-State Mater. Adv. Technol. 176 (2011) 1207–1212. doi:10.1016/j.mseb.2011.06.015.

[23] Chih-Ming Chen, Yu-Chun Hsu, Sheng-Jye Cherng, Effects of annealing conditions on the properties of TiO$_2$/ITO-based photoanode and the photovoltaic performance of dye-sensitized solar cells, J. Alloys Compd. 509 (2011) 872–877. doi:10.1016/j.jallcom.2010.09.118.

[24] J. Spannhake, A. Helwig, G. Müller, G. Faglia, G. Sberveglieri, T. Doll, T. Wassner, M. Eickhoff, SnO$_2$:Sb - A new material for high-temperature MEMS heater applications: Performance and limitations, Sensors Actuators, B Chem. 124 (2007) 421–428. doi:10.1016/j.snb.2007.01.004.

[25] T. Minami, T. Miyata, T. Yamamoto, Stability of transparent conducting oxide films for use at high temperatures, J. Vac. Sci. Technol. A. 17 (1999) 1822. doi:10.1116/1.581897.

[26] S. Ngamsinlapasathian, T. Sreethawong, Y. Suzuki, S. Yoshikawa, Doubled layered ITO/SnO$_2$ conducting glass for substrate of dye-sensitized solar cells, Sol. Energy Mater. Sol. Cells. 90 (2006) 2129–2140. doi:10.1016/j.solmat.2005.12.005.

[27] T. Jäger, B. Bissig, M. Döbeli, A.N. Tiwari, Y.E. Romanyuk, Thin films of SnO$_2$:F by reactive magnetron sputtering with rapid thermal post-annealing, Thin Solid Films. 553

(2014) 21–25. doi:10.1016/j.tsf.2013.12.038.

[28] M.T.S. Nair, L. Guerrero, O.L. Arenas, P.K. Nair, Chemically deposited copper oxide thin films: structural, optical and electrical characteristics, Appl. Surf. Sci. 150 (1999) 143–151. doi:10.1016/S0169-4332(99)00239-1.

[29] M.T.S. Nair, C. López-Mata, O. GomezDaza, P.K. Nair, Copper tin sulfide semiconductor thin films produced by heating SnS–CuS layers deposited from chemical bath, Semicond. Sci. Technol. 18 (2003) 755–759. doi:10.1088/0268-1242/18/8/306.

[30] A. Diéguez, A. Romano-Rodríguez, A. Vilà, J.R. Morante, The complete Raman spectrum of nanometric SnO_2 particles, J. Appl. Phys. 90 (2001) 1550–1557. doi:10.1063/1.1385573.

[31] K.N. Yu, Y. Xiong, Y. Liu, C. Xiong, Microstructural change of nano-SnO_2 grain assemblages with the annealing temperature, Phys. Rev. B. 55 (1997) 2666–2671. doi:10.1103/PhysRevB.55.2666.

[32] L. Sangaletti, L.E. Depero, B. Allieri, F. Pioselli, E. Comini, G. Sberveglieri, M. Zocchi, Oxidation of Sn thin films to SnO_2. Micro-Raman mapping and x-ray diffraction studies, J. Mater. Res. 13 (1998) 2457–2460. doi:10.1557/JMR.1998.0343.

[33] B. Eifert, M. Becker, C.T. Reindl, M. Giar, L. Zheng, A. Polity, Y. He, C. Heiliger, P.J. Klar, Raman studies of the intermediate tin-oxide phase, Phys. Rev. Mater. 1 (2017) 14602. doi:10.1103/PhysRevMaterials.1.014602.

[34] S.S. Lekshmy, G.P. Daniel, K. Joy, Microstructure and physical properties of sol gel derived SnO_2:Sb thin films for optoelectronic applications, Appl. Surf. Sci. 274 (2013) 95–100. doi:10.1016/j.apsusc.2013.02.109.

[35] A.A. Yadav, S.C. Pawar, D.H. Patil, M.D. Ghogare, Properties of (200) oriented, highly conductive SnO_2 thin films by chemical spray pyrolysis from non-aqueous medium: Effect of antimony doping, J. Alloys Compd. 652 (2015) 145–152. doi:10.1016/j.jallcom.2015.08.197.

[36] S. Gupta, B.C. Yadav, P.K. Dwivedi, B. Das, Microstructural, optical and electrical investigations of Sb-SnO_2 thin films deposited by spray pyrolysis, Mater. Res. Bull. 48 (2013) 3315–3322. doi:10.1016/j.materresbull.2013.05.001.

[37] L. Guo, M. Zhao, D. Zhuang, Q. Gong, H. Tan, M. Cao, L. Ouyang, A study on phase transformation of SnO_x thin films prepared by reactive magnetron sputtering, Mater. Sci. Semicond. Process. 46 (2016) 35–38. doi:10.1016/j.mssp.2015.10.008.

[38] A. Seko, A. Togo, F. Oba, I. Tanaka, Structure and stability of a homologous series of tin oxides, Phys. Rev. Lett. 100 (2008) 45702. doi:10.1103/PhysRevLett.100.045702.

[39] P. Sarker, M.N. Huda, Understanding the thermodynamic pathways of SnO-to-SnO_x phase

transition, Comput. Mater. Sci. 111 (2016) 359–365.
doi:10.1016/j.commatsci.2015.09.041.

[40]   C. Körber, J. Suffner, A. Klein, Surface energy controlled preferential orientation of thin films, J. Phys. D. Appl. Phys. 43 (2010) 55301. doi:10.1088/0022-3727/43/5/055301.

[41]   H. Kim, A. Piqué, Transparent conducting Sb-doped SnO_2 thin films grown by pulsed-laser deposition, Appl. Phys. Lett. 84 (2004) 218. doi:10.1063/1.1639515.

[42]   A. Rahal, A. Benhaoua, C. Bouzidi, B. Benhaoua, B. Gasmi, Effect of antimony doping on the structural, optical and electrical properties of SnO_2 thin films prepared by spray ultrasonic, Superlattices Microstruct. 76 (2014) 105–114. doi:10.1016/j.spmi.2014.09.024.

[43]   F. Zhang, Y. Lian, M. Gu, J. Yu, T.B. Tang, Static and dynamic disorder in metastable phases of tin oxide, J. Phys. Chem. C. 121 (2017) 16006–16011.
doi:10.1021/acs.jpcc.7b04477.

[44]   J. Boltz, D. Koehl, M. Wuttig, Low temperature sputter deposition of SnO_x:Sb films for transparent conducting oxide applications, Surf. Coatings Technol. 205 (2010) 2455–2460. doi:10.1016/j.surfcoat.2010.09.048.

[45]   M.P.S. Rana, F. Singh, K. Joshi, S. Negi, R.C. Ramola, Influence of electronic excitations on structural, optical and electrical properties of undoped and antimony doped tin oxide thin films, Thin Solid Films. 616 (2016) 34–42. doi:10.1016/j.tsf.2016.07.070.

[46]   W.M. Kim, J.S. Kim, J.H. Jeong, J.K. Park, Y.J. Baik, T.Y. Seong, Analysis of optical band-gap shift in impurity doped ZnO thin films by using nonparabolic conduction band parameters, Thin Solid Films. 531 (2013) 430–435. doi:10.1016/j.tsf.2013.01.078.

[47]   K.G. Saw, N.M. Aznan, F.K. Yam, S.S. Ng, S.Y. Pung, New insights on the Burstein-Moss shift and band gap narrowing in indium-doped zinc oxide thin films, PLoS One. 10 (2015) e0141180. doi:10.1371/journal.pone.0141180.

[48]   S. Yu, L. Ding, C. Xue, L. Chen, W.F. Zhang, Transparent conducting Sb-doped SnO_2 thin films grown by pulsed laser deposition, J. Non. Cryst. Solids. 358 (2012) 3137–3140. doi:10.1016/j.jnoncrysol.2012.09.009.

[49]   C. Guillén, J. Herrero, Structural and plasmonic characteristics of sputtered SnO_2:Sb and ZnO:Al thin films as a function of their thickness, J. Mater. Sci. 51 (2016) 7276–7285. doi:10.1007/s10853-016-0010-9.

[50]   I.H. Kim, J.H. Ko, D. Kim, K.S. Lee, T.S. Lee, J. -h. Jeong, B. Cheong, Y.-J. Baik, W.M. Kim, Scattering mechanism of transparent conducting tin oxide films prepared by magnetron sputtering, Thin Solid Films. 515 (2006) 2475–2480.
doi:10.1016/j.tsf.2006.07.020.

[51]   E. Shanthi, A. Banerjee, V. Dutta, K.L. Chopra, Annealing characteristics of tin oxide

films prepared by spray pyrolysis, Thin Solid Films. 71 (1980) 237–244. doi:10.1016/0040-6090(80)90160-1.

[52] A. Albar, Z. Wang, H.N. Alshareef, U. Schwingenschlögl, Formation of metallic states between insulating SnO and SnO_2, Adv. Mater. Interfaces. 2 (2016) 1500334. doi:10.1002/admi.201500334.

[53] A. Albar, H.A. Tahini, U. Schwingenschlögl, Metallicity at interphase boundaries due to polar catastrophe induced by charge density discontinuity, NPG Asia Mater. 10 (2018) e469. doi:10.1038/am.2017.236.

[54] X.Q. Pan, L. Fu, Oxidation and phase transitions of epitaxial tin oxide thin films on (1012) sapphire, J. Appl. Phys. 89 (2001) 6048–6055. doi:10.1063/1.1368865.

[55] B. Bissig, T. Jäger, L. Ding, A.N. Tiwari, Y.E. Romanyuk, Limits of carrier mobility in Sb-doped SnO_2 conducting films deposited by reactive sputtering, APL Mater. 3 (2015) 62802. doi:10.1063/1.4916586.

[56] I.A. Alagdal, A.R. West, Oxygen non-stoichiometry, conductivity and gas sensor response of SnO_2 pellets, J. Mater. Chem. A. 3 (2015) 23213–23219. doi:10.1039/C5TA05818J.

[57] M. Chen, Z.L. Pei, X. Wang, Y.H. Yu, X.H. Liu, C. Sun, L.S. Wen, Intrinsic limit of electrical properties of transparent conductive oxide films, J. Phys. D. Appl. Phys. 33 (2000) 2538–2548. doi:10.1088/0022-3727/33/20/304.

[58] H.C. Lee, O.O. Park, Behaviors of carrier concentrations and mobilities in indium-tin oxide thin films by DC magnetron sputtering at various oxygen flow rates, Vacuum. 77 (2004) 69–77. doi:10.1016/j.vacuum.2004.08.006.

[59] H.E. Ruda, Compensation and transport characteristics of n-ZnTe, J. Phys. D. Appl. Phys. 24 (1991) 1158–1162. doi:10.1088/0022-3727/24/7/021.

[60] C. Guillén, J. Herrero, Nanocrystalline copper sulfide and copper selenide thin films with p-type metallic behavior, J. Mater. Sci. 52 (2017) 13886–13896. doi:10.1007/s10853-017-1489-4.

Table 1: Summary of the optical properties (visible transmittance, band-gap energy) and electrical characteristics (carrier concentration, mobility, conductivity) obtained for the various deposition conditions and different heating temperatures.

Samples	O_{pp} (%)	target	T_{vis} (%)	E_g (eV)	N (cm^{-3})	μ (cm^2/Vs)	σ (S/cm)
as-grown	18	Sn	83	2.96	$7.0*10^{11}$	20	$1.9*10^{-6}$
		Sn:Sb	70	2.68	$6.0*10^{12}$	28	$2.6*10^{-5}$
	24	Sn	97	3.70	$5.1*10^{17}$	6	$4.9*10^{-1}$
		Sn:Sb	91	3.74	$4.9*10^{19}$	1	$8.8*10^{0}$
250 °C heated	18	Sn	86	2.98	$2.3*10^{12}$	49	$1.6*10^{-5}$
		Sn:Sb	75	2.85	$2.3*10^{12}$	46	$1.7*10^{-4}$
	24	Sn	97	3.57	$9.2*10^{19}$	13	$1.7*10^{2}$
		Sn:Sb	92	3.76	$2.1*10^{20}$	8	$2.7*10^{2}$
450 °C heated	18	Sn	86	3.32	$6.1*10^{18}$	6	$5.7*10^{0}$
		Sn:Sb	78	2.92	$2.3*10^{20}$	3	$1.2*10^{2}$
	24	Sn	96	4.00	$4.1*10^{16}$	3	$2.5*10^{-2}$
		Sn:Sb	92	3.82	$4.6*10^{20}$	2	$1.6*10^{2}$

19

Highlights:

SnO$_2$ and SnO$_2$:Sb are prepared by reactive sputtering on unheated substrates.

Conductivity in amorphous SnO$_2$ is dominated by oxygen vacancies.

Optimal Sb$_{Sn}$ incorporation is achieved by crystallization above 400 ℃.

Coexistence with intermediate oxides allows the formation of cation interstitials.

Sb-doping and intermediate oxides reduce the average visible transmittance.